Available online at www.sciencedirect.com
SCIENCE DIRECT
Medical Engineering & Physics 28 (2006) 613–628
Medical Engineering & Physics
www.elsevier.com/locate/medengphy

A concentrated parameter model for the human cardiovascular system including heart valve dynamics and atrioventricular interaction

Theodosios Korakianitis *, Yubing Shi

Department of Mechanical Engineering, University of Glasgow, Glasgow G12 8QQ, UK

Received 8 March 2005; received in revised form 29 September 2005; accepted 6 October 2005

Abstract

Numerical modeling of the human cardiovascular system has always been an active research direction since the 19th century. In the past, various simulation models of different complexities were proposed for different research purposes. In this paper, an improved numerical model to study the dynamic function of the human circulation system is proposed. In the development of the mathematical model, the heart chambers are described with a variable elastance model. The systemic and pulmonary loops are described based on the resistance–compliance–inertia concept by considering local effects of flow friction, elasticity of blood vessels and inertia of blood in different segments of the blood vessels. As an advancement from previous models, heart valve dynamics and atrioventricular interaction, including atrial contraction and motion of the annulus fibrosus, are specifically modeled. With these improvements the developed model can predict several important features that were missing in previous numerical models, including regurgitant flow on heart valve closure, the value of *E/A* velocity ratio in mitral flow, the motion of the annulus fibrosus (called the KG diaphragm pumping action), etc. These features have important clinical meaning and their changes are often related to cardiovascular diseases. Successful simulation of these features enhances the accuracy of simulations of cardiovascular dynamics, and helps in clinical studies of cardiac function.

Keywords: Numerical simulation; Cardiovascular dynamics; Heart valve model; Atrioventricular interaction; Atrial contraction

1. Introduction

Numerical simulation of physiological and pathological changes in the human cardiovascular system has its origin in the 19th century [1], and it has become an active research area in the past decades with the development of computer technology. Various mathematical models have been proposed to study the dynamics of the cardiovascular system. General models in this area can be classified as distributed parameter models and concentrated parameter models. Distributed parameter models are mostly used in investigations of local dynamics in certain parts of the cardiovascular system, including the heart [2], heart valves [3,4] and blood vessels [5], with computational fluid dynamics [2,4], finite element analysis [3], transmission line method [5,6], etc. In contrast, concentrated parameter models are mostly used to study the global response of the circulation system, and although sometimes a local part is studied, the ultimate target of research with concentrated parameter models is still the global response of the system.

Concentrated parameter modeling in the cardiovascular system began with the Windkessel model proposed by Otto Frank in 1899 to model the general resistance and capacitance effects of systemic blood vessels [1,7]. Later, this evolved into: the modified Windkessel model (for instance, [8]); non-linear viscoelastic property study of vessel segments [9]; pressure-dependent description of veins [9,10]; pressure-dependent description of venae cavae [10]; pressure-dependent compliance effect of the arteries [11,12]; variable resistance effect of arterioles [13]. In recent years several fractal models of the blood vessel have been proposed [14,15]. The early discussion on heart models was on whether the characteristics of the ventricle are better described as a pressure driven or a flow-rate driven phenomenon, as referred to by Leefe and Gentle [16]. In the 1970s, Suga et

* Corresponding author. Tel.: +44 141 330 2490; fax: +44 141 330 2480.
E-mail address: t.alexander@mech.gla.ac.uk (T. Korakianitis).

1350-4533/$ – see front matter © 2005 IPEM. Published by Elsevier Ltd. All rights reserved.
doi:10.1016/j.medengphy.2005.10.004

Nomenclature

A	sectional area
AR	area ratio
C	compliance
CQ	flow coefficient
DT	time step
E	elastance
F	force
I	inertial moment of rotating
K	coefficient
l	displacement of the annulus fibrosus
L	inertance
M	mass
P	pressure
Q	flow-rate
r	radius
R	resistance
t	time
T	heart period
V	volume
θ	rotating angle of valve leaflet

Subscripts

0	initial value; offset value; value for unstressed condition
ao	aortic valve
d	diastolic phase
e	elastance action
ea	elastance of atrium
ev	elastance of ventricle
f	frictional action
la	left atrium
lv	left ventricle
max	maximum value
mi	mitral valve
min	minimum value
p	effect of pressure force
par	pulmonary arterioles
pas	pulmonary artery sinus
pat	pulmonary artery
pav	right annulus fibrosus
pcp	pulmonary capillary
po	pulmonary aortic valve
pvc	pulmonary venae cavae
pvn	pulmonary vein
pwb	beginning of P wave in ECG
pww	duration of P wave in ECG
ra	right atrium
rv	right ventricle
s	systolic phase
s1	peak of systolic phase
s2	end of systolic phase
sar	systemic arterioles
sas	systemic aortic sinus
sat	systemic artery
sav	left annulus fibrosus
scp	systemic capillary
st	strain action
sve	systemic venae cavae
svn	systemic vein
ti	tricuspid valve

al. [17] proposed a variable elastance model for the ventricle. This model attracted the attention of most researchers, and it has been widely used from then on [9–11,13,18–34]. Some researchers even extended this model to study the atrial contraction effect [23,26,33]. New activation functions for this model also evolved in recent years [35]. Besides modeling the heart chamber, some researchers also studied intra-ventricular interaction [22,25,26,36], postulating that this crosstalk between the two neighboring ventricles affects the global dynamic response. However, in a critical review Melchior Francois et al. [37] implicitly questioned the importance of intra-ventricular interaction.

Models of neurological regulation in the cardiovascular system have also been developed. Closed-loop regulation models of the cardiovascular system were proposed in which the pressure signal in the baroreceptor was fed back for combined sympathetic and parasympathetic control of the heart rate, ventricle contractility, arteriole resistance and vein tone [10,13,21,26,28–32]. These studies have seen promising applications in areas such as orthostatic response in training of astronauts, study of physiological processes like hemorrhagic shock and so on.

These studies greatly improved our understanding of cardiovascular dynamics, but there are still areas unexplored in the modeling work. One issue is the detailed analysis of heart valve dynamics. In the human heart four heart valves work together to keep the blood flowing in one direction. Heart valve dynamics greatly influence the pressure and flow-rate changes in the heart. In previous investigations these heart valves were mostly modeled as diodes plus a linear or non-linear resistance [20,21,24,33]. This description puts more emphasis on the ideal characteristic of one-way flow in the heart valve, while the more complex aspects of valve dynamics were ignored, so that realistic features of local hemodynamics such as regurgitant flow were not simulated. Žáček and Krause [38] used the concept of a time-dependent drag coefficient to describe the heart valve in their simulation. In their work the drag coefficient is a function of the valve open area, and it approaches infinity when the valve is closed. The drag coefficients were added to the losses of the conduit where the valve was situated. Werner et al. [39] described the valve dynamics by introducing the concept of dead-space volume, which is the volume of fluid contained in the valve region. The dead-space volume is a function of the

valve leaflet opening angle, and the volume is zero when the valve is fully closed. These two models improved heart valve modeling, but the leaflet motion was prescribed instead of computed, so that the blood–leaflet interaction effect, which dominates the leaflet dynamics, was not considered.

Yacoub Magdi et al. [40] studied the aortic outflow and the aortic root, and suggested that aortic flow is a tale of dynamism and crosstalk between the blood and the surrounding structures including sinuses of Valsalva, valve cusps and the contracting ventricle chamber. Besides the contraction motion of the ventricle, the aortic root and valve cusps also have smooth muscles that contribute to the crosstalk. In this complex interaction vortices form in the sinuses of Valsalva. These vortices play an important role in smooth valve opening and closure, and aid coronary flow. This opinion gives a realistic and in-depth description of physiological phenomena in aortic flow.

Due to limitations in research methods and computing facilities, realistic modeling of blood–valve dynamics can only be carried out with considerable simplifications, e.g. by omitting the contraction and elasticity of the valve cusps and aortic root, ignoring the effect of vortices in the sinuses of Valsalva, and considering only the effect of pressure difference and shear stress in the valve. Some research work has been carried out in this direction [41–48,4]. In the current research such distributed parameter description for the valve function is adapted and included within the concentrated parameter study for the overall dynamic model of the circulation system. This helps to simulate the dicrotic notch in aortic pressure, and the regurgitant flow on valve closure, which are important features in revealing pathological and physiological changes in clinical diagnoses. In comparison to previous models that treated the heart valves as diodes combined with resistances, or modeled the valve dynamics but used prescribed leaflet motion, the proposed model improves the accuracy of the simulations.

Another issue is the atrioventricular interaction effect, which was analysed and termed the KG diaphragm by Korakianitis and Grandia [49], because it acts as a diaphragm pump (as opposed to a dividing septum like the atrial septum). Kilner Philip et al. [50] briefly discussed the role of this atrioventricular interaction in their research of asymmetric redirection of flow through the heart. Power [51] modeled this effect with a first-order differential equation in his numerical simulation of systemic circulation. However, in Power's analysis only the pressure difference and the elastic force in the septum were considered, while the active stretching actions of the atrial and ventricular chamber walls were ignored. With Power's model, in the systolic phase the KG diaphragm would bulge into the atrial chamber due to increased ventricular pressure. This result is exactly contrary to what happens under the physiological systole condition, in which the KG diaphragm is pulled into the ventricular chamber due to the active contractile action of the surrounding ventricle wall. In the work reported here, the contribution of the KG diaphragm motion to cardiac dynamics is modeled by including the effect of nearby tissue stress on the KG diaphragm, based on our MRI measurements on a healthy human volunteer.

The current work is a further contribution in cardiovascular system modeling. We present a numerical model of the whole human circulation system which includes several phenomena that were not simulated in previous models. The heart chambers are described with the variable elastance model as proposed by Suga et al. [17]. Features of atrial contraction motion, the pumping effect of the motion of the KG diaphragm and dynamics of the heart valves are specifically included in the proposed model. In our simulations the developed model is solved with a four-stage Runge–Kutta method to study the system response under the action of these features.

2. Method

2.1. MRI measurement of cardiac dynamics

As preliminary experimental study of cardiac dynamics for this work, and in order to provide suitable inputs to the numerical models, we carried out MRI measurements of geometric changes in the four heart chambers of a healthy human subject. The subject was scanned with a 1.5-T Philips Gyroscan ACS-NT MRI system (release 8.1, Philips Medical Systems, Best, The Netherlands) utilizing a five-element cardiac phased array coil. Vectorcardiographic ECG gating equipment was employed for accurate cardiac synchronisation. Survey images were first obtained, and subsequent breath-hold balanced fast field echo (steady-state free precession) cine images were performed in: left heart two chamber; short-axis two chamber; horizontal long axis four-chamber orientations, in order to plan standard planes for cardiac short-axis imaging. In these short-axis measurements 20 slice levels (6 mm thick with zero gap) that spanned from the apex of the ventricles to the cardiac base (including the atria) were captured. At each level, cine imaging was performed using sensitivity encoding parallel acquisition to allow 30 phases per cardiac cycle in a breath-hold, with a field of view of 420 mm and an image matrix of 256×256. The in-plane resolution was 1.6 mm. Similar multi-slice, multiphase cine imaging was performed in transaxial planes with similar parameters. Corroborative phase contrast quantitative flow imaging for flow curves was performed across both the aortic root and right ventricular outflow tract with retrospective ECG gating and a temporal resolution of 35 cardiac phases.

Post-processing consisted of evaluating volume changes for each chamber with cardiac analysis software (EasyVision release 4.2, Philips Medical Systems) to delineate the endocardial contours of the chambers. Functional parameters were derived, i.e. end diastolic volume, end systolic volume, stroke volume and volumetric ejection fraction. The individual images were also saved in TIFF format and exported to a CAD program SolidEdge (Version 14.0, Electronic Data

Fig. 1. Short-axis MRI slice in diastolic phase.

System Corporation, TX, USA) for reconstruction of the three-dimensional geometries of the heart chambers.

The motion trend of the KG diaphragm observed from the MRI measurements provided the basis for qualitative comparison with the results predicted in the current numerical simulation. The maximum and minimum displacements of the KG diaphragm were used for parameter setting in modeling the atrioventricular interaction effect. As measurement of the KG diaphragm motion is not currently a standard procedure in clinical practice, point to point tracking of the two-dimensional or reconstructions of the three-dimensional KG diaphragm motion during the heart cycle was not automatically supported in the MRI system. The motion trend of the KG diaphragm was estimated (with computer graphics applications) from the MRI movies, and used for qualitative comparison with the simulation results. This measurement of the KG diaphragm pumping motion and pumping action deserves further investigations in future clinical and modeling research.

Fig. 1 shows one of the MRI short-axis images in the end diastolic phase. Solid-edge images of the lower portions of the corresponding three-dimensional geometry of the left and right ventricles reconstructed from the MRI image data are shown in Fig. 2. Fig. 3 gives the volume change of the left ventricle during a heart cycle, and agrees very well with other experimental measurements of the volume trace presented, for instance, in [52,53], and that shown in physiology textbooks, for instance, [54–57]. From these we constructed the typical volume response illustrated in Fig. 4(c) clearly demonstrating local volume increase due to atrial contraction. Fig. 4(c) already covers the main features of Fig. 3, and Fig. 4 gives other additional details of the pressure and flow-rate changes in a typical heart cycle. Therefore, in the discussion of the results comparisons are made mainly with Fig. 4, while the volume change in Fig. 3 and the motion of the

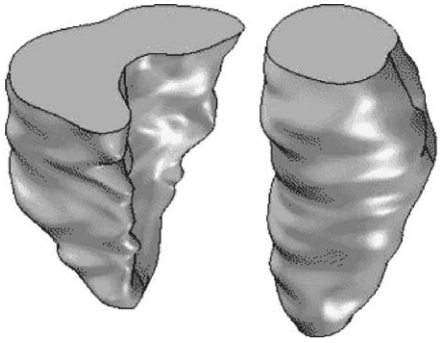

Fig. 2. Solid-edge images of the lower portions of ventricle geometries in diastole, reconstructed from MRI measurements.

KG diaphragm observed in the MRI measurements are also referred to when appropriate. Image sequences in these MRI measurements revealed that due to interaction between the atrium and the ventricle, the KG diaphragm moves along the long axis of the adult heart for about 0.02–0.03 m in each heart cycle. The area around the aorta does not move significantly during the heart cycle, and most of the KG diaphragm motion, and corresponding pumping action, is attributed to motion of the annulus fibrosus around the mitral valve. This motion of the mitral-valve annulus fibrosus of the KG diaphragm contributes about 8–12 ml to the volume change of each heart chamber, which is more than 10% of the total 70 ml stroke volume. This pumping action of the KG diaphragm affects the physiological response of the heart, and is specifically modeled in the numerical approach presented in this paper.

2.2. Conceptual illustration of general cardiac response

The mathematical model must be developed while considering the general features of the cardiovascular system response it tries to simulate. Fig. 4 illustrates the general conceptual trends of the physiological changes in the systemic circulation loop, including pressure, flow-rate and volume variations in one heart cycle. Fig. 4 is constructed based on

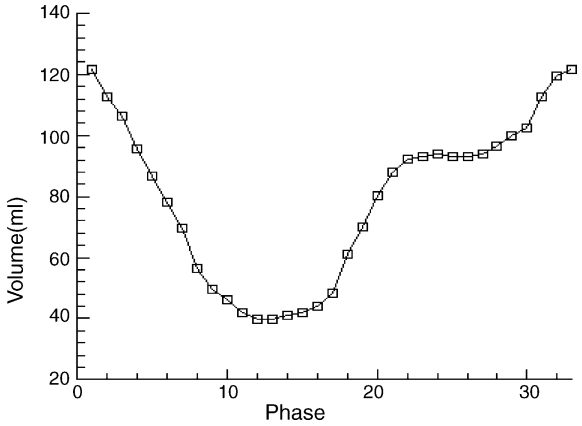

Fig. 3. Volume change of left ventricle measured from MRI data.

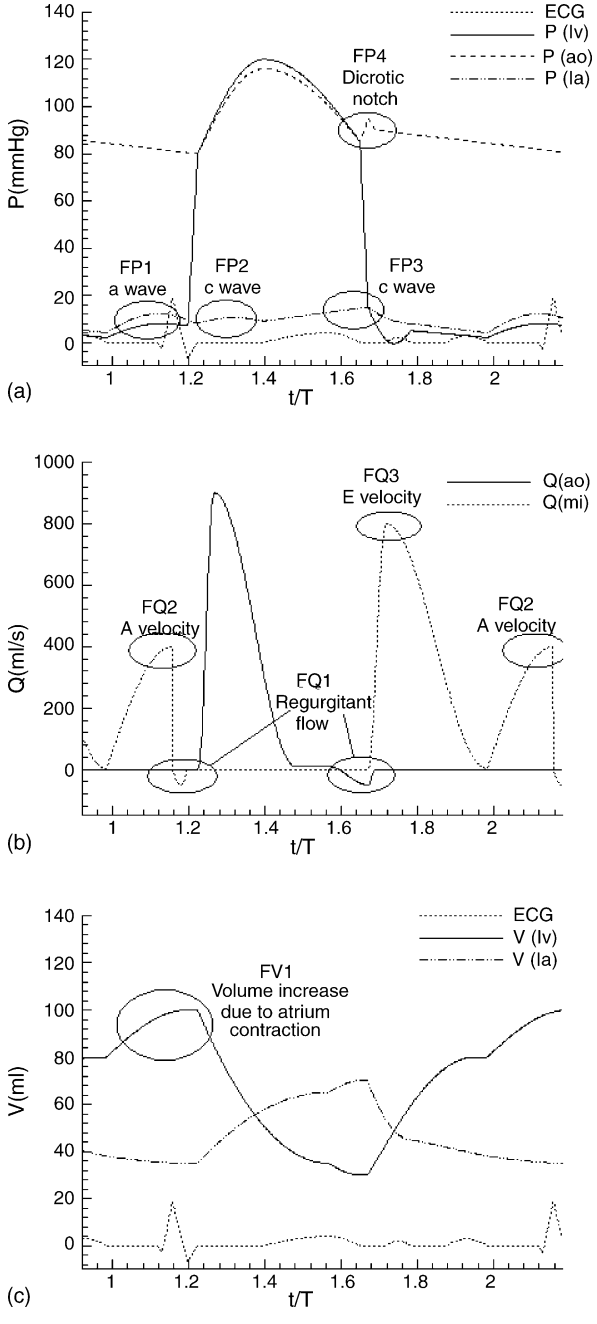

Fig. 4. (a–c) Illustration of the systemic loop response of the cardiovascular system during a typical healthy-heart cycle.

general knowledge of cardiovascular physiology published in textbooks and journals [1,54–59]. Besides the normal trends and parameter ranges, several important features are specifically included in Fig. 4, which are mostly absent from the simulation results of former researchers. In Fig. 4(a) illustrating the pressure changes, features FP1, FP2 and FP3 correspond to the 'a' wave, 'c' wave and 'v' wave in atrial pressure, respectively. Feature FP4 is the dicrotic notch in aortic pressure, generated by aortic valve closure. In the flow-rate changes in Fig. 4(b), feature FQ1 corresponds to regurgitant flow in the mitral and aortic valves at the end stages of diastole and systole. Features FQ2 is the *A* velocity peak in mitral flow due to atrial contraction in late diastole, and FQ3 is the *E* velocity peak due to initial filling flow to the left ventricle in early diastole. In the volume changes in Fig. 4(c), feature FV1 represents the volume jump in late diastolic phase due to atrial contraction, which was also observed in the MRI measurement results illustrated in Fig. 3.

2.3. Mathematical model

Components of the whole circulation system are modeled as illustrated in Fig. 5 in three main parts: heart, systemic circulation loop and pulmonary circulation loop. The heart is modeled as a four-chamber pump with variable elastance and four heart valves that control the blood flow direction. The systemic and pulmonary circulation loops are each separated into aortic sinus/pulmonary artery sinus, artery, arteriole, capillary and vein segments. In every segment the individual component is modeled by considering the local resistance to blood flow, elasticity of blood vessels and inertia of blood. The combined effect of venule, vein and vena cava is modeled as the vein segment. The artery segment represents the general characteristics of both the main and smaller arteries. The aortic sinus is separated from the artery to facilitate estimation of pressure response in the aortic arch.

2.3.1. Ventricle

Basic ventricular characteristics are described with the pressure-volume relation with the widely used Suga et al.'s variable elastance model [17], in which the ventricular pressure is described as a linear function of the chamber volume and the chamber elastance. The chamber volume is decided by the flow-rate difference between the inlet and the outlet of the chamber, while the chamber elastance varies in a heart cycle representing the action of the heart muscle.

The instantaneous volume change in the left ventricle is equal to the flow-rate difference between mitral and aortic valves:

$$\frac{\mathrm{d}V_{\mathrm{lv}}}{\mathrm{d}t} = Q_{\mathrm{mi}} - Q_{\mathrm{ao}} \tag{1}$$

The time-varying ventricle elastance is a function of the characteristic elastance ($E_{\mathrm{lv,s}}$ and $E_{\mathrm{lv,d}}$) and an activation function $\bar{e}_{\mathrm{lv}}(t)$:

$$e_{\mathrm{lv}}(t) = E_{\mathrm{lv,d}} + \frac{E_{\mathrm{lv,s}} - E_{\mathrm{lv,d}}}{2} \cdot \bar{e}_{\mathrm{lv}}(t) \tag{2}$$

The activation function $\bar{e}_{\mathrm{lv}}(t)$ describes the contraction and the relaxation changes in the ventricular muscle. Ottesen and Danielsen [35] compared several forms of activation functions in their work and investigated their applicability. Generally, these activation functions have only slight differences in shapes due to different assumptions used in model derivation. A commonly used activation function is adopted

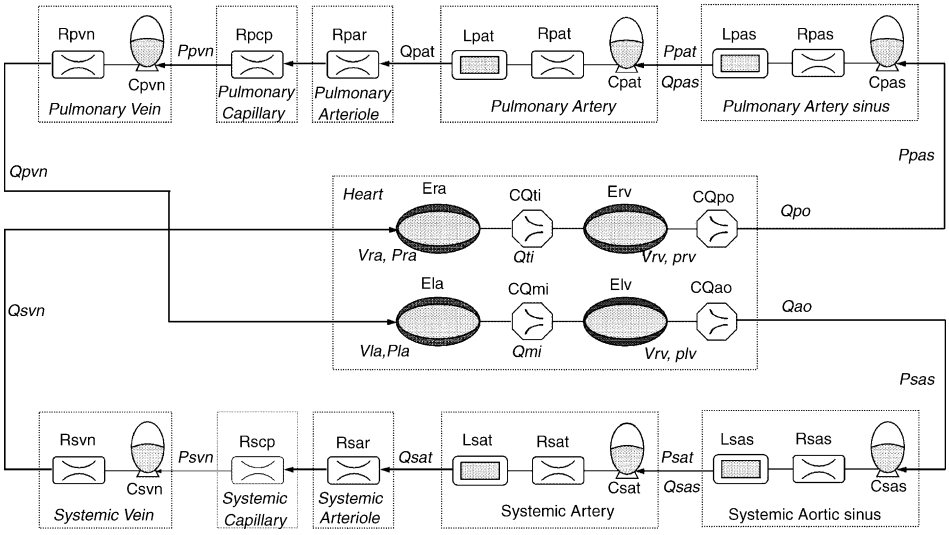

Fig. 5. Schematic of the circulation system model.

here:

$$\bar{e}_{\mathrm{lv}}(t) = \begin{cases} 1 - \cos\left(\dfrac{t}{T_{\mathrm{s1}}}\pi\right), & 0 \le t < T_{\mathrm{s1}} \\ 1 + \cos\left(\dfrac{t - T_{\mathrm{s1}}}{T_{\mathrm{s2}} - T_{\mathrm{s1}}}\pi\right), & T_{\mathrm{s1}} \le t < T_{\mathrm{s2}} \\ 0, & T_{\mathrm{s2}} \le t < T \end{cases} \tag{3}$$

The left ventricular elastance change in a typical heart cycle obtained using this activation function is illustrated in Fig. 6. The pressure in the left ventricle is then derived from the instantaneous volume and elastance values in the ventricle:

$$P_{\mathrm{lv}} = P_{\mathrm{lv},0} + e_{\mathrm{lv}}(V_{\mathrm{lv}} - V_{\mathrm{lv},0}) \tag{4}$$

The motion of the annulus fibrosus also affects volume changes in the heart, as described in the following sections. The model for the right ventricle is similar to that for the left side, except the values of parameters are different.

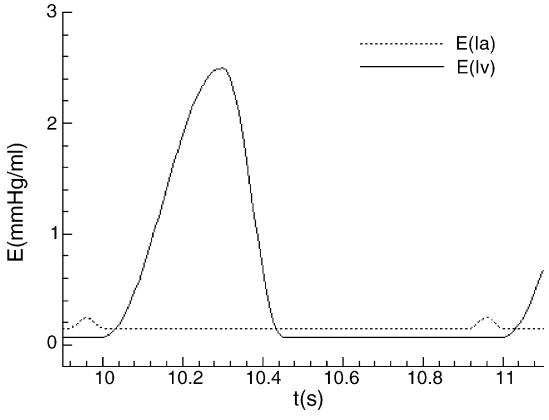

Fig. 6. Elastance change in the left ventricle and left atrium during a typical heart cycle.

2.3.2. Atrium

Following the P wave in the ECG signal, the atrium contracts and leads to a rapid rise in the ventricular end diastolic volume and pressure. This effect is sometimes called the "atrial kick", which contributes about 20–30% of ventricular filling volume and reflects the "booster pump" function of the atrium [54,55]. Features FP1, FQ2 and FV1 in Fig. 4 reflect the influence of this action. In those previous studies that ignored atrial contraction, these features are missing.

In describing the left atrium, the modeling process is very similar to that for the left ventricle. Again, Suga et al.'s variable elastance model [17] is adopted, while the values of parameters and the form of the activation function are adapted to represent the dynamic changes in the atrium. To analyse the effect of atrial contraction, the system models both with and without consideration of atrial contraction are adopted. When the atrial contraction effect is ignored, the atrium elastance $e_{\mathrm{la}}(t)$ is set to a constant value of $E_{\mathrm{la,min}}$. When the atrial contraction effect is considered, the atrium elastance is represented with variable elastance model, as used by [24,27,33,38]:

$$e_{\mathrm{la}}(t) = E_{\mathrm{la,min}} + \frac{E_{\mathrm{la,max}} - E_{\mathrm{la,min}}}{2} \cdot \bar{e}_{\mathrm{la}}(t) \tag{5}$$

in which the atrium activation function is set as:

$$\bar{e}_{\mathrm{la}}(t) = \begin{cases} 0, & 0 \le t < T_{\mathrm{pwb}} \\ 1 - \cos\left(\dfrac{t - T_{\mathrm{pwb}}}{T_{\mathrm{pww}}} 2\pi\right), & T_{\mathrm{pwb}} \le t < T_{\mathrm{pwb}} + T_{\mathrm{pww}} \\ 0, & T_{\mathrm{pwb}} + T_{\mathrm{pww}} \le t < T \end{cases} \tag{6}$$

The corresponding elastance change in the left atrium in a typical heart cycle obtained using this activation function is illustrated in Fig. 6. In the right atrium the governing

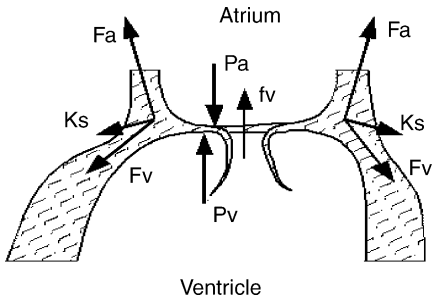

Fig. 7. Forces acting on the KG diaphragm in the vicinity of the mitral valve.

equations are similar, except the values of parameters can be different.

2.3.3. Atrioventricular interaction

The KG diaphragm is a soft tissue which includes the annulus fibrosus and the four heart valves. In the native heart the KG diaphragm undergoes periodic displacement into the atrial or ventricular chambers under the combined action of several forces. Fig. 7 illustrates a portion of the KG diaphragm and the forces acting on it in the vicinity of the mitral valve. These include: the pressure force $(P_{lv} - P_{la})A_{sav}$ which is due to the pressure difference across the valves and surrounding tissue; the tissue strain forces $F_{st,la}$ and $F_{st,lv}$ from both the atrium and the ventricle sides that act on the annulus fibrosus base; the frictional force $K_{f,sav}(dl/dt)$ from blood flow; the elastic force $K_{e,sav}l$ due to the elasticity of the KG diaphragm [49]. The KG diaphragm displacement l is decided by the balance of all these forces. The MRI measurements of heart kinetics in several heart cycles in an adult native healthy heart show that in the systolic phase the KG diaphragm moves into the ventricular chamber, and in end diastolic phase it moves into the atrium (due to atrial contraction). The total displacement along the long axis of the heart is about 0.02–0.03 m.

Based on Newton's second law of motion, in the left heart the KG diaphragm dynamics are governed by:

$$M_{sav}\frac{d^2l}{dt^2} = F_{st,la} - F_{st,lv} + (P_{lv} - P_{la})A_{sav} - K_{f,sav}\frac{dl}{dt} - K_{e,sav}l \quad (7)$$

Here, the diaphragm neutral position is assigned to the location where both the atrium and the ventricle are in their unstressed status, and motion into the atrium is assigned as positive displacement.

Based on the MRI measurements, as a first approximation it is assumed that tissue strain is a linear function of the corresponding elasticity status of the chamber muscle. These effects are modeled by:

$$F_{st,la} = K_{e,la} \cdot e_{la} \quad (8)$$

$$F_{st,lv} = K_{e,lv} \cdot e_{lv} \quad (9)$$

Thus, in the left heart the KG diaphragm dynamic equation is:

$$M_{sav}\frac{d^2l}{dt^2} = K_{st,la} \cdot e_{la} - K_{st,lv} \cdot e_{lv} + (P_{lv} - P_{la})A_{sav} - K_{f,sav}\frac{dl}{dt} - K_{e,sav}l \quad (10)$$

The motion of the KG diaphragm redefines the location of the atrioventricular boundary at each time instant and introduces volume changes to the two chambers:

$$V_{lv} = V_{lv} + A_{sav} \cdot l \quad (11)$$

$$V_{la} = V_{la} - A_{sav} \cdot l \quad (12)$$

In the right heart KG diaphragm dynamics are modeled in a similar way.

2.3.4. Heart valves

Most prior studies have modeled heart valves as resistance components in the fully open or fully closed position, while the dynamics of the opening and closing processes were not considered. There were some who considered the opening and closing processes, such as Žáček and Krause [38], and Werner et al. [39], but they used prescribed valve motion, which neglected the blood–leaflet interaction effect, and thus the results were enormously compromised. In those previous works that ignored the heart valve dynamics, features FP4 (dicrotic notch) and FQl (regurgitant flow in the valves) are missing from the system predicted response.

In the physical system heart valve dynamics are dominated by the blood–leaflet interaction effect [41,44–46,4]. Full description of this effect needs detailed three-dimensional distributed parameter modeling of the pulsatile flow field around the valve and the valve–leaflet deformation/motion (such as with CFD studies). Previous studies on the blood–leaflet interaction effect [41–48,4] are mostly case specific, and cannot be used for overall dynamic modeling of the whole cardiovascular system as illustrated in Fig. 5. As a novel contribution, this paper makes a compromise between the detailed three-dimensional study and the simplified diode-like description of the valve, using a concentrated parameter method to describe the blood–leaflet interaction effect. For this modeling purpose, the heart valve is simplified as follows: a nominal leaflet opening angle is used as an average of the variation of angular position in the different parts of the elastic leaflet; the detailed pressure and velocity distributions in the valve are rounded and replaced with the averaged pressure and flow-rate before and after the valve. The nominal leaflet opening angle is calculated by solving the governing differential equation for the leaflet dynamics, which takes into account the contribution of the blood flow, while the corresponding leaflet motion also drives the local pressure and flow-rate changes around the valve. This concentrated parameter model of the blood–leaflet interaction effect is less detailed than three-dimensional distributed parameter studies, but is an advancement over the diode models, and it

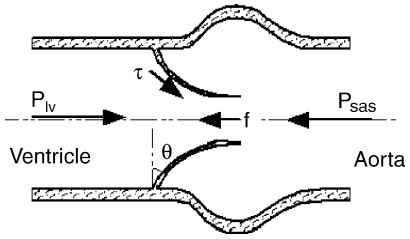

Fig. 8. Illustration of typical forces acting on a heart valve leaflet.

satisfies the need of the present paper to model the overall cardiovascular system.

In the current model the basic pressure–flow relation in the aortic valve is described with an orifice model as usually used in fluid mechanics [60]:

$$Q_{ao} = \begin{cases} CQ_{ao} \cdot AR_{ao} \cdot \sqrt{P_{lv} - P_{sas}}, & P_{lv} \geq P_{sas} \\ CQ_{ao} \cdot AR_{ao} \cdot \sqrt{P_{sas} - P_{lv}}, & P_{lv} < P_{sas} \end{cases} \quad (13)$$

while the valve opening AR_{ao} is derived in two ways. In the simplified model, like that of most prior studies, the valve opening switches between 0 and 1 corresponding to fully closed and fully open positions, depending on which side of the valve has higher pressure:

$$AR_{ao} = \begin{cases} 1, & P_{lv} \geq P_{sas} \\ 0, & P_{lv} < P_{sas} \end{cases} \quad (14)$$

In our complete model, the circular valve opening is a function of the angular position of the valve leaflets, as illustrated in Fig. 8:

$$AR_{ao} = \frac{\pi[r_{ao}(1 - \cos\theta)]^2}{\pi[r_{ao}(1 - \cos\theta_{max})]^2} = \frac{(1 - \cos\theta)^2}{(1 - \cos\theta_{max})^2} \quad (15)$$

In Eq. (15), θ is the leaflet opening angle. Zero degree for θ corresponds to the fully closed leaflet position, and the maximum opening angle corresponds to the fully open leaflet position. θ is computed by considering the various factors that affect the leaflet motion. These include: the moment due to the pressure difference across the valve; the moment generated by the shear stress on the leaflet due to fluid flow; the moment produced by the frictional force; the moment generated by the vortex near the valve leaflet surface, as shown in Fig. 8. Based on the CFD results of De Hart et al. [41–43] and Shi et al. [4], the shear stress force is much smaller than the pressure force acting on the leaflet, so the shear stress acted on the valve is neglected. The effect of the vortex in the heart valve is an open question and its contribution is still under investigation. Some researchers proposed that the vortices influence the valve closing process [40,61], but this argument needs further validation, and it is the subject of future investigations. Thus, in this paper the vortex effect is also neglected. Based on these considerations the following governing equation for the aortic leaflet motion is derived:

$$I_{ao} \cdot \frac{d^2\theta}{dt^2} = k_{p,ao} \cdot (P_{lv} - P_{sas}) A_{ao} \cos\theta - k_{f,ao} \cdot \frac{d\theta}{dt} \quad (16)$$

The parameters needed in the model are reduced from three (I_{ao}, $k_{p,ao}$ and $k_{f,ao}$) to two ($K_{P,ao}$ and $K_{f,ao}$) by dividing through with I_{ao} and simplifying the equation in the model to:

$$\frac{d^2\theta}{dt^2} = K_{p,ao} \cdot (P_{lv} - P_{sas}) \cos\theta - K_{f,ao} \cdot \frac{d\theta}{dt} \quad (17)$$

The consideration of valve dynamics helps to describe the regurgitant flow in the valve, thus improving the accuracy of the simulation. Modeling of the remaining three valves is implemented in the same way, except the values of model parameters can be different.

2.3.5. Blood circulation loops

In modeling the various components of systemic circulation, depending on detailed local flow conditions, the frictional loss, elastance and blood inertia are modeled as resistance, compliance and inductance effects, following the classical idea of electric-fluid analog. The systemic circulation loop is divided into five parts: aortic sinus, artery, arterioles, capillary and vein. The aortic sinus and artery are quite elastic, and the flow is pulsatile in these segments, so that all the resistance, compliance and inductance effects must be considered. The arterioles and capillaries are dominated by the resistance effect. Veins function to collect and store blood; thus, resistance and compliance effects are considered in the vein model.

Pressure and flow-rate oscillations are experienced in the aortic sinus due to the local tissue elastance and result in important flow features related to coronary flow. The pressure is governed by:

$$\frac{dP_{sas}}{dt} = \frac{Q_{ao} - Q_{sas}}{C_{sas}} \quad (18)$$

and the flow-rate is:

$$\frac{dQ_{sas}}{dt} = \frac{P_{sas} - P_{sat} - R_{sas} \cdot Q_{sas}}{L_{sas}} \quad (19)$$

The pressure and flow-rate changes in the artery are similar to that in the aortic sinus. As arterioles and capillaries are both considered as pure resistance units, their effects are integrated with the artery as resistance units. Thus, the pressure equation is:

$$\frac{dP_{sat}}{dt} = \frac{Q_{sas} - Q_{sat}}{C_{sat}} \quad (20)$$

and the flow-rate equation is:

$$\frac{dQ_{sat}}{dt} = \frac{P_{sas} - P_{svn} - (R_{sat} + R_{sar} + R_{scp})Q_{sat}}{L_{sat}} \quad (21)$$

The systemic vein is modeled as a compliance combined with a resistance. In the vein the pressure is:

$$\frac{dP_{svn}}{dt} = \frac{Q_{sat} - Q_{svn}}{C_{svn}} \quad (22)$$

and the flow-rate is governed by:

$$Q_{svn} = \frac{P_{svn} - P_{ra}}{R_{svn}} \quad (23)$$

The pulmonary loop model is similar to that of the systemic loop, with different values for system parameters.

2.4. System parameters

Values for the physiological parameters are usually difficult to measure, and they change from person to person. This is a common problem in medical and biomedical studies. To minimize the potential influence of the values of these parameters on the results, great care was taken to assign values to these physiological variables based on data in widely referred papers and textbooks. Where no such data were available, great effort was made to find the reasonable range of values for the variables from the open literature, and the suitable values were then chosen from the range.

Most hemodynamic variables in the above model are assigned values derived from the open literature. Chamber elastance values are assigned as shown in Table 1, based on the parameter selection in [10,21,27,28]. Key parameters for the systemic and pulmonary loops are shown in Table 2, based on [10,13,27,28].

Coefficients for KG diaphragm motion and heart valve dynamics are estimated based on physiological conditions observed in our MRI measurements and found in textbooks. In modeling the KG diaphragm motion, the diameter of the annulus fibrosus of the mitral valve is assumed to be 25 mm, and the thickness of the annulus fibrosus is assumed to be 1 mm. Taking the tissue density to be 0.8 kg/m^3, the annulus fibrosus has a sectional area of 4.7×10^{-4} m^2 and mass of 4.0×10^{-4} kg. During the heart cycle the annulus fibrosus is under continuous reciprocating motion around its neutral position. Our MRI measurements indicate that the annulus fibrosus has a displacement of about 0.02–0.03 m during the heart cycle, and in the diastolic phase the annulus fibrosus is stretched into the atrium chamber with a displacement of about 0.003 m. The coefficients in the governing equations for KG diaphragm motion are then derived, and listed in Table 3. The coefficients of the valve dynamics model were estimated by considering the normal flow-rate and pressure loss in the valves and the relative contribution of various factors that affect the valve motion, thus producing near physiological valve motion as described in the literature [41–48,4]. The corresponding parameter settings are included in Table 4.

Other parameters such as duration of systole, the beginning and duration of the P wave, the time step of simulation, etc., were chosen based on general information published in physiological textbooks [54,55]. Table 5 shows values for these parameters.

3. Results

A program is developed in C language to conduct numerical simulations of the dynamic changes in the heart chambers and the blood vessels. The equations are integrated in time with the four-stage Runge–Kutta method. For ease of comparison of results the heart period is chosen to be 1 s. The simulation reaches periodic solution after four to five heart cycles. To facilitate discussion of results, in all cases the converged solution of the 11th period, from the 10th to the 11th second, is presented in the figures. In this paper, the simplified system response is compared to the response of the overall proposed model. In the companion paper changes to the simplified system response as each new feature of the model is added are presented and discussed [62].

First, the simulation is carried out using the simplified model. In the simplified model all the components are modeled in the conventional way. The ventricles are described with variable elastance model in the form of Eqs. (l)–(4). The systemic and pulmonary loops are modeled with the RLC concept as described by Eqs. (18)–(23). The atria are treated as constant elastance chambers with atrial elastance set to value of $E_{la,min}$. The KG diaphragm motion is neglected, and heart valves are modeled as a diode with non-linear resistance effect, described by Eqs. (13) and (14). In carrying out the simulation, values for the parameters are assigned as illustrated in Tables 1, 2 and 5. The corresponding responses in the cardiovascular system with this simplified model, including pressure, flow-rate and volume changes in a typical heart cycle in the left and right parts of the heart, are shown in Fig. 9(a–f).

The simulation results shown in Fig. 9 agree well with the conceptual drawings in Fig. 4 in the sense that they predict the general trends and parameter ranges. The left ventricular pressure is in the range of 0–120 mmHg, and the aortic pressure changes between 80 mmHg and 120 mmHg. Periodic peak flows exist in the mitral and aortic flow-rates, with average flow-rate of about 5 l/min. The left ventricular volume change is approximately from 50 ml to 120 ml, with a stroke volume of 70 ml. Even though in this simplified model the atria are modeled as chambers with constant elastance, they still accumulate blood during systole, so feature FP3 for the 'v' wave is observed in the atrial pressure change in Fig. 9(a and d), but with decreased amplitude (due to the decreased elastance in this simplified model). The *E* velocity peak is present in mitral and tricuspid flow, but as the *A* velocity peak is absent (due to neglecting atrial contraction), the ratio of early to late velocities (*E*/*A*) cannot be evaluated. Also, due to neglecting atrial contraction, features FP1 for the 'a' wave, FP2 for the 'c' wave, FQ2 for the *A* velocity peak and FV1 for the volume jump are missing from the system response. Because valve dynamics are not considered in the

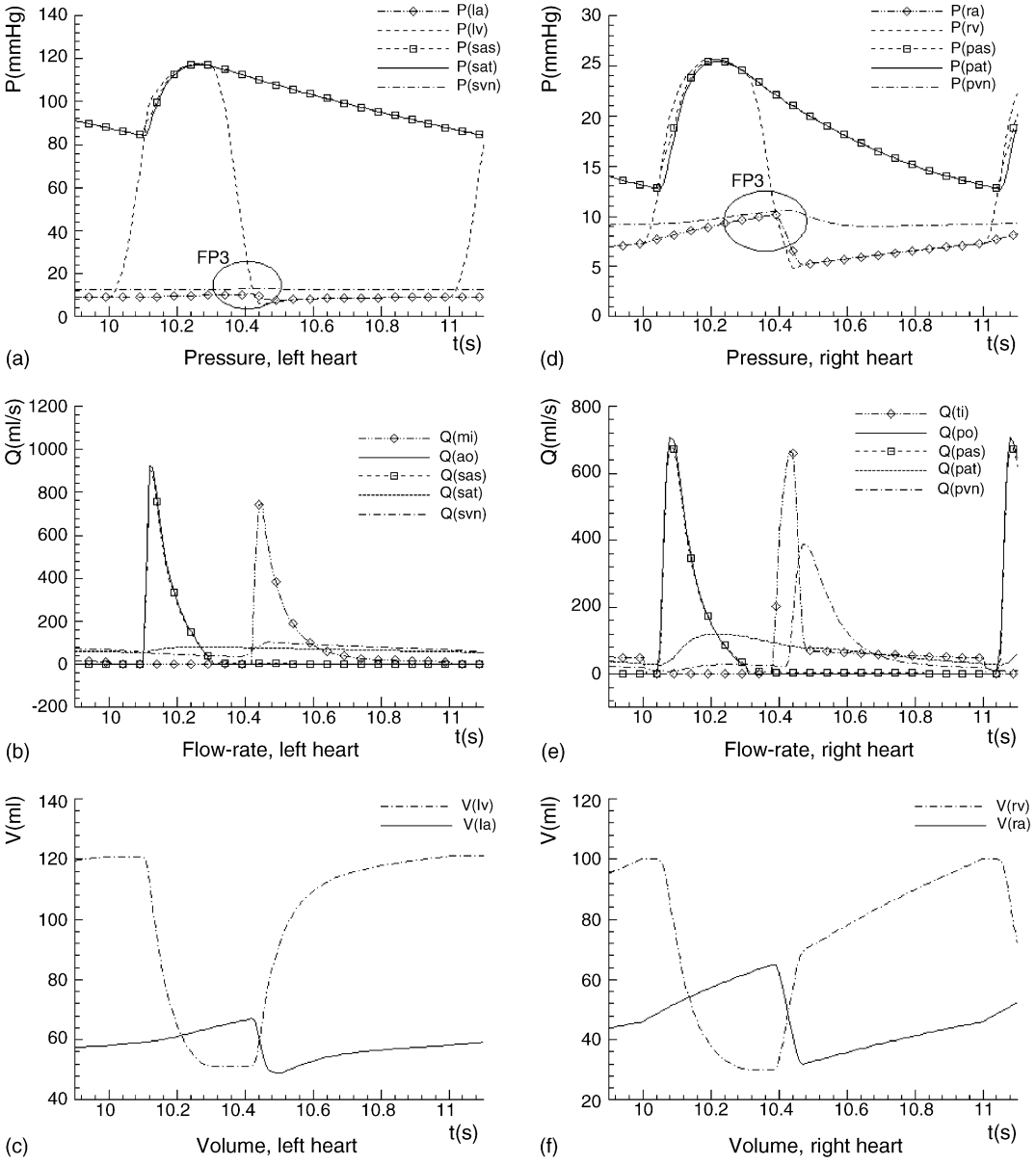

Fig. 9. (a–f) Response with the simplified model.

simplified model, features FP4 for the dicrotic notch in the aortic pressure and pulmonary vein pressure, and FQ1 for valve regurgitant flow, are also missing from this simplified system response.

To study the effects of atrial contraction, KG diaphragm motion and heart valve dynamics on the system response, simulation is carried out to investigate the system response under the combined action of these features. In this case, Eqs. (5) and (6) for variable atrial elastance are used to replace the constant atrial elastance value of $E_{\mathrm{la,min}}$ in the simplified model; Eq. (10) for KG diaphragm dynamics and Eqs. (11) and (12) for correction of atrial and ventricular volumes are combined in the modeling; Eq. (14) in the simplified model is replaced with Eqs. (15) and (17) to include heart valve dynamics. Related system parameter settings are listed in Tables 1–5. Results for KG diaphragm displacement, heart valve angle changes and corresponding pressure, flow-rate and volume changes in a typical heart cycle are illustrated in Figs. 10–12.

Fig. 10 illustrates the displacement of the KG diaphragm in the left heart during a heart cycle. Here, diaphragm displacement refers to the motion of the root of the annulus fibrosus with respect to its neutral position (when the atrium and ventricle are in the unstressed condition). Comparison of Fig. 10 with Fig. 6 for elastance changes in the left atrium and ventricle suggests that motion of the KG diaphragm generally follows the changes of the atrial and ventricular elasticity, and thus the corresponding changes in tissue stress. This means that although the motion of the KG diaphragm is also affected by pressure changes in the heart chambers, the dominant

Table 1
Parameters for the heart

Part	Parameter	Value
Left heart	CQ_{ao} (ml/(s mmHg$^{0.5}$))	350
	CQ_{mi} (ml/(s mmHg$^{0.5}$))	400
	$E_{lv,s}$ (mmHg/ml)	2.5
	$E_{lv,d}$ (mmHg/ml)	0.1
	$P_{lv,0}$ (mmHg)	1.0
	$V_{lv,0}$ (ml)	5.0
	$E_{la,max}$ (mmHg/ml)	0.25
	$E_{la,min}$ (mmHg/ml)	0.15
	$P_{la,0}$ (mmHg)	1.0
	$V_{la,0}$ (ml)	4.0
Right heart	CQ_{po} (ml/(s mmHg$^{0.5}$))	350
	CQ_{ti} (ml/(s mmHg$^{0.5}$))	400
	$E_{rv,s}$ (mmHg/ml)	1.15
	$E_{rv,d}$ (mmHg/ml)	0.1
	$P_{rv,0}$ (mmHg)	1.0
	$V_{rv,0}$ (ml)	10
	$E_{ra,max}$ (mmHg/ml)	0.25
	$E_{ra,min}$ (mmHg/ml)	0.15
	$P_{ra,0}$ (mmHg)	1.0
	$V_{ra,0}$ (ml)	4.0

factor of diaphragm motion is the tissue elasticity. In the systolic phase, due to increased tissue stress in the ventricle, the KG diaphragm is dragged into the ventricle and moves towards the apex of the heart, with the peak displacement reaching −0.0291 m from the neutral position. In the diastolic phase, decrease of ventricular elastance causes the tissue stress in the ventricle to become smaller than that in the atrium, so that the KG diaphragm moves back towards the atrium, and the peak displacement is 0.0032 m.

Table 2
Parameters for the blood vessels

Branch	Parameter	Value
Systemic circulation	C_{sas} (ml/mmHg)	0.08
	R_{sas} (mmHg s/ml)	0.003
	L_{sas} (mmHg s^2/ml)	0.000062
	C_{sat} (ml/mmHg)	1.6
	R_{sat} (mmHg s/ml)	0.05
	L_{sat} (mmHg s^2/ml)	0.0017
	R_{sar} (mmHg s/ml)	0.5
	R_{scp} (mmHg s/ml)	0.52
	R_{svn} (mmHg s/ml)	0.075
	C_{svn} (ml/mmHg)	20.5
	C_{svc} (ml/mmHg)	1.5
	V_{lvo} (ml)	500
Pulmonary circulation	C_{pas} (ml/mmHg)	0.18
	R_{pas} (mmHg s/ml)	0.002
	L_{pas} (mmHg s^2/ml)	0.000052
	C_{pat} (ml/mmHg)	3.8
	R_{pat} (mmHg s/ml)	0.01
	L_{pat} (mmHg s^2/ml)	0.0017
	R_{par} (mmHg s/ml)	0.05
	R_{pcp} (mmHg s/ml)	0.25
	R_{pvn} (mmHg s/ml)	0.006
	C_{pvn} (ml/mmHg)	20.5
	C_{pvc} (ml/mmHg)	1.5
	V_{rv0} (ml)	400

Table 3
Parameters for KG diaphragm motion modeling

Part	Parameter	Value
Left heart	$K_{st,la}$ (m/(s^2 mmHg))	2.5
	$K_{st,lv}$ (m/(s^2 mmHg))	20.0
	$K_{f,sav}$ (s^{-1})	0.0004
	$K_{e,sav}$ (s^{-2})	9000.0
	M_{sav} (kg)	0.0004
	A_{sav} (m^2)	0.00047
Right heart	$K_{st,ra}$ (m/(s^2 mmHg))	2.5
	$K_{st,rv}$ (m/(s^2 mmHg))	20.0
	$K_{f,pav}$ (s^{-1})	0.0004
	$K_{e,pav}$ (s^{-2})	9000.0
	M_{pav} (kg)	0.0004
	A_{pav} (m^2)	0.00047

Table 4
Parameters for variable valve opening model

Part	Parameter	Value
Systemic part	$K_{p,ao}$ (m/(s^2 mmHg))	5500
	$K_{f,ao}$ (s^{-1})	50
	$K_{p,mi}$ (m/(s^2 mmHg))	5500
	$K_{f,mi}$ (s^{-1})	50
	$K_{p,sv}$ (m/(s^2 mmHg))	5500
	$K_{f,sv}$ (s^{-1})	50
Pulmonary part	$K_{p,po}$ (m/(s^2 mmHg))	5500
	$K_{f,po}$ (s^{-1})	50
	$K_{p,ti}$ (m/(s^2 mmHg))	5500
	$K_{f,ti}$ (s^{-1})	50
	$K_{p,pv}$ (m/(s^2 mmHg))	5500
	$K_{f,pv}$ (s^{-1})	50

Table 5
Additional parameters

Parameter	Value
DT (s)	0.0001
T (s)	1.0
T_{s1} (s)	0.30
T_{s2} (s)	0.45
T_{pwb} (s)	0.92
T_{pww} (s)	0.09

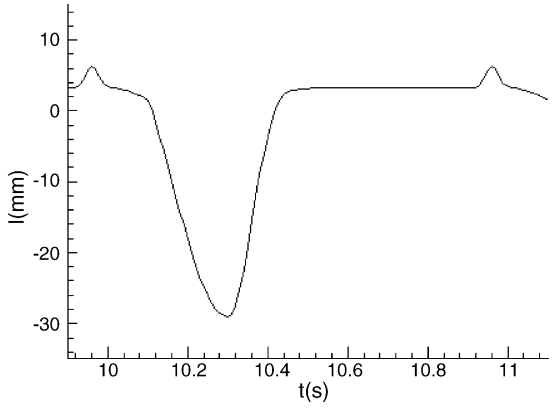

Fig. 10. KG diaphragm motion in left heart when all the features of atrial contraction, KG diaphragm motion and heart valve dynamics are considered.

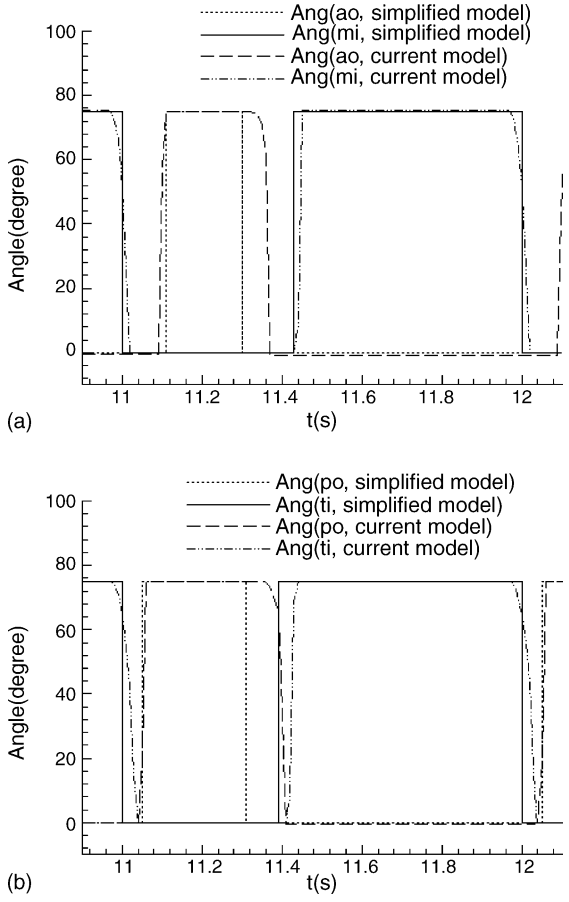

Fig. 11. (a and b) Comparison of changes of heart valve leaflet angular position (opening) between the simplified model, and the model in which all the features of atrial contraction, KG diaphragm motion and heart valve dynamics are considered.

In end diastole, due to atrial contraction (and the corresponding increase in atrial elastance), displacement of the KG diaphragm reaches the peak value of 0.0061 m. This motion trend generally matches that observed in the MRI measurements.

Fig. 11 compares the valve opening changes simulated with the simplified model and the proposed new model. In the results predicted by the simplified model, the valves open and close abruptly, driven by the local pressure difference across the valves. With the proposed model the opening changes become smoother with the introduction of the valve dynamics model. The exact moments of valve opening and closing also change, and the effect is more pronounced in the response of the pulmonary and tricuspid valves. From Fig. 11 it is observed that the valve opening and closing processes take about 0.1 s. Comparing the valve motions in the right heart to those in the left heart, it is found that the pulmonary valve opens about 0.15 s earlier and closes about 0.1 s later than the aortic valve, and the tricuspid valve opens about 0.05 s earlier and closes about 0.05 s later than the mitral valve. This is closely related to the lower pressure range in the pulmonary loop and the slower pressure change rate in the right ventricle. The atrial pressures in the left and right heart are similar; thus, the slower rise in pressure in the right ventricle induces the later closing of the tricuspid valve. The earlier opening of the tricuspid and pulmonary valves, and the later closing of the pulmonary valve are the results of the combined actions of the lower pressures in the pulmonary loop, and slower rate of changes on pressure in the right ventricle.

Fig. 12 compares the pressure, flow-rate and volume changes predicted by the simplified model (as illustrated in Fig. 9) with that predicted by the proposed model. In Fig. 12 trace lines with triangular tick marks and with a prime (′) in the legends for pressure, flow-rate and volume traces are the response when the features of atrial contraction, KG diaphragm motion and heart valve dynamics are considered, while those trace lines without the triangular marks and the prime in the legends represent the response with the simplified model (of Fig. 9).

In the pressure response in Fig. 12(a and d), it is found that features FPl (‘a’ wave in atrial pressure waveform), FP3 (‘v’ wave in atrial pressure) and FP4 (dicrotic notch) are clearly demonstrated. These features require inclusion of atrial contraction and valve dynamics in the simulation. Feature FP2 of ‘c’ wave is not obvious in the atrial pressure waveform, due to its minor physiological effect and due to neglecting leaflet elasticity in the valve model. The combined effect of atrial contraction, valve dynamics and KG diaphragm motion greatly decreases the peak left ventricular systolic pressure from 117.4 mmHg to 102.7 mmHg, thus decreasing the aortic pressure by about 20 mmHg all over the heart cycle. The combined effect of these features does not change the peak right ventricular pressure much, while the pressure in the pulmonary artery is decreased by about 0.8–3.1 mmHg in the diastolic phase. Left and right atrial pressures are slightly elevated in the heart cycle. Pressure drops in the right heart are much smaller than that in the left heart. This is due to the highly distensible blood vessels, and thus the greater compliance in the pulmonary loop, which buffers the pressure pulsation significantly.

All three features of FQ1 (regurgitant flow), FQ2 (*A* velocity effect in mitral/tricuspid flow) and FQ3 (*E* velocity effect in mitral/tricuspid flow) are simulated in the flow-rate response in Fig. 12(b and e). Compared to the simplified model, under the combined action of atrial contraction, KG diaphragm motion and heart valve dynamics, in both systemic and pulmonary loops the peak values of flow-rate through the heart valves are increased. In the aortic valve the value increases from 920.8 ml/s to 1183.6 ml/s; in the mitral valve from 744.6 ml/s to 851.4 ml/s; in the pulmonary valve from 695.5 ml/s to 879.4 ml/s; in the tricuspid valve from 665.5 ml/s to 911.4 ml/s. The *E*/*A* ratios are about 2 in both left and right heart.

Fig. 12(c and f) shows that due to the combined action of atrial contraction, KG diaphragm motion and heart valve dynamics, the atrial volume is shifted upward slightly, except for a local trough in late diastole due to atrial contraction, while ventricular volume is prominently increased in

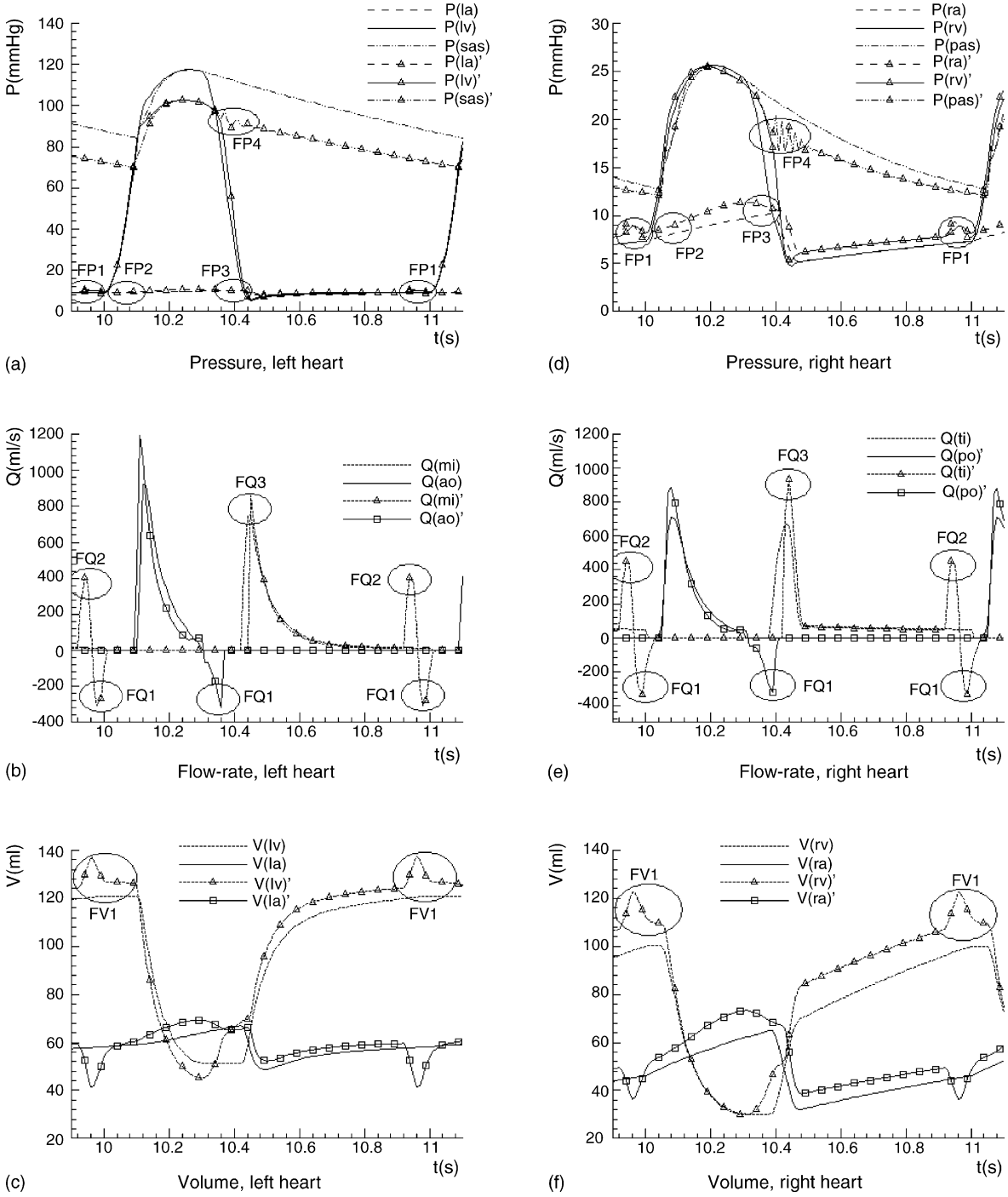

Fig. 12. (a–f) Response when all the features of atrial contraction, KG diaphragm motion and heart valve dynamics are considered.

the diastolic phase, and decreased in the systolic phase; thus, the diastolic–systolic volume difference in the ventricle increases by about 30%, when compared to the simplified model. However, not all of this 30% increase changes into increase of stroke volume. Considering the contribution of atrial contraction and KG diaphragm motion, the real increase in stroke volume here is estimated to be only about 20% of the ventricular diastolic–systolic volume difference, and the remaining part is consumed on the extra volume load caused by the regurgitant flow in heart valves. Feature FV1, corresponding to the increase in ventricular volume due to atrial contraction, can be clearly observed in the volume response. However, due to regurgitant flow in the mitral and tricuspid valves caused by heart valve dynamics, this volume increase is compromised in the late stage of diastole.

4. Discussion

Numerical modeling of the human cardiovascular system is an active research area due to its increasing use in physiological and pathological studies. Various models have been developed to address different aspects of cardiovascular dynamics. Most of these models concentrate on one detailed aspect of the overall system to suit specific application requirements, for instance, foetal circulation [23,24], response to orthostatic stress [21], isocapnic hypoxia [30,31], etc. Although the above are useful for the specific applications, the model presented in this paper takes a different approach and emphasizes dynamics within the four chambers of the heart. At the same time the proposed cardiac dynamics model can still be coupled to any model of the whole of the circulation loop. These circulation loop models can include simpler models of the systemic or pulmonary circulation loops, or in a more comprehensive model they can include local elaborate models of elements of the circulation loops such as renal flow, hepatic flow, cerebral flow, etc. Specifically, the cardiac dynamics model presented can be used to provide the input to the whole network of downstream blood vessels, which can be as simplified or as detailed as the specific study requires.

Previous cardiac models consider various features in cardiac dynamics, such as atrial contraction [23,26,33] and intra-ventricular interaction [22,25,26,36], but do not include the combined effects of atrioventricular interaction and heart valve dynamics. Based on clinical MRI measurements, the present paper takes into account the atrial and ventricular tissue stretching effect, and results in realistic description of the motion of the atrioventricular annulus fibrosus. Previous models of heart valve dynamics modeled the valve as a diode–resistance combination, or introduced concepts of time-varying drag coefficient or dead-space volume while using prescribed valve leaflet motion. The present paper improves on previous models by directly considering the simplified blood–leaflet effect that governs the valve leaflet motion.

The combination of models in this paper, including the combination of atrial contraction, atrioventricular interaction and heart valve leaflet dynamics, successfully predicts a realistic description of key details of cardiac dynamics. By comparing the simulation results with the conceptual drawing for cardiovascular dynamics extracted from textbooks, it is observed that main cardiac-flow dynamic features in the pressure changes with time, flow-rate changes with time and volume changes with time in the four chambers of the heart that were missing in previous work are realistically predicted in the current work. In the pressure response, features FP1, FP2 and FP3 for ‘a’, ‘c’ and ‘v’ waves in atrial pressure are revealed with the combination of models for atrial contraction, ventricular contraction and atrioventricular interaction. These features are more prominent in the pulmonary loop than in the systemic loop due to the relative amplitude of the atrial pressure variation to ventricular pressure variation in the two loops. Feature FP4 for the dicrotic notch is also manifested with the improved heart valve dynamics model, which is missing in most previous models. In the flow-rate response, the new heart valve dynamics model contributes to revealing feature FQl for regurgitant flow in the heart valves, which is also missing in most previous models. Features FQ2 for *A* velocity, FQ3 for *E* velocity and the *E*/*A* ratio in the mitral/tricuspid flow are also illustrated with the combined model for atrial contraction and atrioventricular interaction. Usually, the above features are not mentioned in previous works. Modeling of heart valve dynamics also approximates aspects of the valve leaflet angular position, and through that of the valve opening and closing process, as illustrated in Fig. 11. Details of feature FV1, some of which were observed in the MRI measurements, and others that appear in physiology books, were simulated. Successful simulation of these features in the pressure, flow-rate and volume response has important physiological meaning, and may have implications for improvements in future clinical practice. Delicate changes in these features often herald the potential, or even the occurrence, of certain cardiovascular diseases. For example, certain changes in the features of FQl, FQ2 and FQ3 may indicate heart valve stenosis or incompetence, and diminishing of feature FV1 may hint atrial fibrillation. Some details of FV1 shown in the computations (Fig. 12) are not evident in the measurements of Fig. 3. Improvements in MRI, echocardiography and other clinical techniques, and their companion software, may be required in order to clearly measure in clinical practice some features observed in the numerical results such as the computed details of FV1 in Fig. 12. In turn, these enhanced clinical measurements will provide data for calibration of the parameters of the numerical model, so that future numerical predictions simulate better the more accurate future clinical measurements.

There are two possible limitations in the current model. First is that in modeling the atrioventricular interaction effect, as a first approximation a linear tissue stress–elasticity relationship is assumed. In future work an improved model should be used, based on experimental results of tissue properties in that area, which are likely to result in a non-linear stress–elasticity tissue relationship. Such a model would improve detailed aspects of the predictions of the model, such as details of the motion of the atrioventricular interaction and valve leaflets, but it will not change the overall nature of the results. The second limitation is in the modeling of heart valve dynamics, due to neglecting the flow–vortex effect. According to the literature, neglecting the vortex effect in the valve dynamics model will cause over-estimation of regurgitant flow. The vortex effect will be investigated in future work.

5. Conclusions

In this paper, a new cardiovascular system model is developed to simulate human circulation dynamics. In the model, the heart is modeled as a four-chamber pump with

variable elasticity. As enhancement from previous models, new models for atrioventricular interaction motion and heart valve dynamics are developed. Based on MRI measurements of cardiac dynamics, motion of the atrioventricular annulus fibrosus, which is acting as a diaphragm pump called the KG diaphragm, is considered in the model, and a linear tissue stress–elasticity constitutive relation is assumed for the atrial and ventricular chambers. Motion of the atrioventricular interaction ring area (KG diaphragm) is modeled by considering the various factors of pressure difference across the diaphragm, frictional force and tissue stress in the atrial and ventricular chambers. Based on previous CFD studies, heart valve dynamics is considered in the model. In modeling heart valve dynamics, the non-linear pressure–flow-rate relation for flow through an orifice is used, and the valve leaflet motion is modeled based on Newton's second law by considering the flow-induced pressure difference across the valve and the frictional force from tissue movement. The shear stress on the leaflet is neglected in the current work, based on previous results of CFD studies. The systemic and pulmonary loops are each modeled as segments of aortic sinus/pulmonary artery sinus, artery, arteriole, capillary and vein, with the combined effects of flow resistance, blood vessel elasticity and blood inertia modeled for each segment based on local flow characteristics.

Simulation results show that, with consideration of atrial contraction and the introduction of new models for the atrioventricular motion and heart valve dynamics, the simulation accuracy is greatly improved. Important physiological characteristics in the cardiac response such as dicrotic notch, regurgitant flow and *E*/*A* ratio are realistically simulated in the current work, while they were mostly missing in previous numerical models. Detailed numerical analysis on the effect of these new features to the cardiac response is presented in a companion paper [62].

Acknowledgment

The authors thank Dr. Gilis Roditi of Glasgow Royal Infirmary, who provided the MRI data from a healthy adult volunteer.

References

[1] Nichols Wilmer W, O'Rourke Michael F. McDonald's blood flow in arteries: theoretical, experimental and clinical principles. 3rd ed. Edward Arnold; 1990.

[2] Baccani B, Domenichini F, Pedrizzetti G, Tonti G. Fluid dynamics of the ventricular filling in dilated cardiomyopathy. J Biomech 2002;35:665–71.

[3] Cacciola G, Peters GWM, Schreurs PJG. A three-dimensional mechanical analysis of a stentless fibre-reinforced aortic valve prothesis. J Biomech 2000;33:521–30.

[4] Shi YB, Zhao Y, Yeo JH, Hwang NHC. Numerical simulation of opening process in a bileaflet mechanical heart valve under pulsatile flow condition. J Heart Valve Dis 2003;12:245–56.

[5] Einav S, Aharoni S, Manoach M. Exponentially tapered transmission line model of the arterial system. IEEE Trans Biomed Eng 1988;35(5):333–9.

[6] Myers LJ, Capper WL. A transmission line model of the human foetal circulation system. Med Eng Phys 2002;24:285–94.

[7] Noordergraaf A. Circulatory system dynamics. Academic Press; 1978.

[8] Sharp MK, Dharmalingam RK. Development of a hydraulic model of the human systemic circulation. ASAIO J 1999;45:334–8.

[9] Barnea O, Moore Thomas W, Dubin Stephen E, Jaron D. Cardiac energy considerations during intraaortic ballon pumping. IEEE Trans Biomed Eng 1990;37(2):170–81.

[10] Lu K, Clark Jr JW, GhorBel FH, Ware DL, Bidani A. A human cardiopulmonary system model applied to the analysis of the valsalva maneuver. Am J Physiol Heart Circ Physiol 2001;281:H2661–79.

[11] Berger David S, Li John K-J. Temporal relation between left ventricular and arterial system elastances. IEEE Trans Biomed Eng 1992;39(4):404–10.

[12] Li John K-J, Cui T, Drzewiecki Gary M. A nonlinear model of the arterial system incorporating a pressure-dependent compliance. IEEE Trans Biomed Eng 1990;37(7):673–8.

[13] Ursino M. Interaction between carotid baroregulation and the pulsating heart: a mathematical model. Am J Physiol Heart Circ Physiol 1998;275(44):H1733–47.

[14] Brown Donald J. Input impedance and reflection coefficient in fractal-like models of asymmetrically branching compliant tubes. IEEE Trans Biomed Eng 1996;43(7):715–22.

[15] Grasman J, Brascamp JW, Van Leeuwen JL, Van Putten B. The multifractal structure of arterial trees. J Theor Biol 2003;220:75–82.

[16] Leefe SE, Gentle CR. A review of the in vitro evaluation of conduit-mounted cardiac valve prostheses. Med Eng Phys 1995;17:497–506.

[17] Suga H, Sagawa K, Shoukas Artin A. Load independence of the instantaneous pressure-volume ratio of the canine left ventricle and effects of epinephrine and heart rate on the ratio. Circ Res 1973;XXXII(March):314–22.

[18] Barnea O. Mathematical analysis of coronary autoregulation and vascular reserve in closed-loop circulation. Comput Biomed Res 1994;27:261–75.

[19] Burkhoff D, Alexander Jr J, Schipke J. Assessment of Windkessel as a model of aortic input impedance. Am J Physiol Heart Circ Physiol 1988;255(24):H742–53.

[20] Drzewiecki G, Wang J-J, Li John K-J, Kedem J, Weiss H. Modeling of mechanical dysfunction in regional stunned myocardium of the left ventricle. IEEE Trans Biomed Eng 1996;43(12):1151–63.

[21] Heldt T, Shim Eun B, Kamm Roger D, Mark Roger G. Computational modeling of cardiovascular response to orthostatic stress. J Appl Physiol 2002;92:1239–54.

[22] Olansen JB, Clark JW, Khoury D, Ghorbel F, Bidani A. A closed-loop model of the canine cardiovascular system that includes ventricular interaction. Comput Biomed Res 2000;33:260–95.

[23] Pennati G, Migliavacca F, Dubini G, Pietrabissa R, de leval Marc R. A mathematical model of circulation in the presence of the bidirectional cavopulmonary anastomosis in children with a univentricular heart. Med Eng Phys 1997;19(3):223–34.

[24] Pennati G, Bellotti M, Fumerco R. Mathematical modelling of the human foetal cardiovascular system based on Doppler ultrasound data. Med Eng Phys 1997;19(4):327–35.

[25] Santamore William P, Burkhoff D. Hemodynamic consequences of ventricular interaction as assessed by model analysis. Am J Physiol Heart Circ Physiol 1991;260(29):H146–57.

[26] Sun Y, Beshara M, Lucariello Richard J, Chiaramida Salvatore A. A comprehensive model for right–left heart interaction under the influence of pericardium and baroreflex. Am J Physiol Heart Circ Physiol 1997;272(41):H1499–515.

[27] Thomas James D, Zhou J, Greenberg N, Bibawy G, McCarthy Patrik M, VanDervoort Pieter M. Physical and physiological determinants

of pulmonary venous flow: numerical analysis. Am J Physiol Heart Circ Physiol 1997;272(41):H2453–65.
[28] Ursino M. A mathematical model of the carotid baroregulation in pulsating conditions. IEEE Trans Biomed Eng 1999;46(4):382–92.
[29] Ursino M, Fiorenzi A, Belardinelli E. The role of pressure pulsatility in the carotid baroreflex control: a computer simulation study. Comput Biol Med 1996;26(4):297–314.
[30] Ursino M, Magosso E. Acute cardiovascular response to isocapnic hypoxia. I. A mathematical model. Am J Physiol Heart Circ Physiol 2000;279:H149–56.
[31] Ursino M, Magosso E. Acute cardiovascular response to isocapnic hypoxia. II. Model validation. Am J Physiol Heart Circ Physiol 2000;279:H166–75.
[32] Ursino M, Magosso E. Role of short-term cardiovascular regulation in heart period variability: a model study. Am J Physiol Heart Circ Physiol 2003;284:H1479–93.
[33] Vollkron M, Shima H, Huber L, Wieselthaler G. Interaction of the cardiovascular system with an implanted rotary assist device: simulation study with a refined computer model. Artif Organs 2002;26(4):349–59.
[34] Yaku H, Goto Y, Futaki S, Ohgoshi Y, Kawaguchi O, Sugu H. Multicompartment model for mechanics and energetics of fibrillating ventricle. Am J Physiol Heart Circ Physiol 1991;260(29):H292–9.
[35] Ottesen JT, Danielsen M. Modelling ventricular contraction with heart rate changes. J Theor Biol 2003;222:337–46.
[36] Chung DC, Niranjan SC, Clark JW, Bidani Jr A, Johnston WE, Zwischenberger JB, et al. A dynamic model of ventricular interaction and pericardial influence. Am J Physiol Heart Circ Physiol 1997;272(41):H2942–62.
[37] Melchior Francois M, Srinivasan RS, Charles John B. Mathematical modeling of human cardiovascular system for simulation of orthostatic response. Am J Physiol Heart Circ Physiol 1992;262(31):H1920–33.
[38] Žáček M, Krause E. Numerical simulation of the blood flow in the human cardiovascular system. J Biomech 1996;19(1):13–20.
[39] Werner J, Böhringer D, Hexamer M. Simulation and prediction of cardiotherapeutical phenomena from a pulsatile model coupled to the Guyton circulation model. IEEE Trans Biomed Eng 2002;49(5):430–9.
[40] Yacoub Magdi H, Kilner Philip J, Birks Emma J, Misfeldn M. The aortic outflow and root: a tale of dynamism and crosstalk. Ann Thorac Surg 1996;68:S37–43.
[41] De Hart J, Paters GWM, Schreurs PJG, Baaijens FPT. A two-dimensional fluid–structure model of the aortic valve. J Biomech 2000;33:1079–88.
[42] De Hart J, Paters GWM, Schreurs PJG, Baaijens FPT. A three-dimensional computational analysis of fluid–structure interaction in the aortic valve. J Biomech 2003;36:103–12.
[43] De Hart J, Baaijens FPT, Paters GWM, Schreurs PJG. A computational fluid–structure interaction analysis of a fiber-reinforced stentless aortic valve. J Biomech 2003;36:699–712.
[44] Kiris C, Kwak D, Rogers S, Chang I-D. Computational approach for probing the flow through artificial heart devices. J Biomech 1997;119(November):452–60.
[45] Lai Yong G, Chandran Krishnan B, Lemmon J. A numerical simulation of mechanical heart valve closure fluid dynamics. J Biomech 2002;35:881–92.
[46] Makhijani Vinod B, Siegel John Jr M, Hwang Ned HC. Numerical study of squeeze-flow in tilting disc mechanical heart valves. J Heart Valve Dis 1996;5:97–103.
[47] Makhijani Vinod B, Siegel John Jr M, Singhal Ashok K. Coupled fluid–structure analysis of bi-leaflet mitral mechanical heart valve dynamics. Adv Bioeng ASME, BED 1996;33:415–6.
[48] Makhijani Vinod B, Yang HQ, Dionne Paul J, Thubrikar Mano J. Three dimensional coupled fluid–structure simulation of pericardial bio-prosthetic aortic valve function. ASAIO J 1997;48:M387–92.
[49] Korakianitis T, Grandia L. Optimized pulsatile flow ventricular assistance device and total artificial heart. United States patent no. US 6,632,169 B2; October 14, 2003.
[50] Kilner Philip J, Yang G-Z, Wilkes AJ, Mohladdin Raad H, Firmin David N, Yacoub Magdi H. Asymmetric redirection of flow through the heart. Nature 2000;404:759–61.
[51] Power HM. Models of electrical and mechanical activity in the heart. In: Linkens D. A., editor. Biological systems, modelling and control, IEE control engineering series, vol. 11. Peter Peregrinus Ltd. on behalf of the Institution of Electrical Engineers; 1979 [chapter 4].
[52] Bowman Andrew W, Frihauf Paul A, Kovács Sándor J. Time-varying effective mitral valve area: prediction and validation using cardiac MRI and Doppler echocardiography in normal subjects. Am J Physiol Heart Circ Physiol 2004;287:H1650–7.
[53] Chen C-H, Nevo E, Fetics B, Nakayama M, Kass David A, Pak Peter H, et al. Comparison of continuous left ventricular volumes by transthoracic two-dimensional digital echo quantification with simultaneous conductance catheter measurements in patients with cardiac diseases. Am J Cardiol 1997;80:756–61.
[54] Guyton Arthur C. Textbook of medical physiology. W.B. Saunders Company; 1986.
[55] West John B. Best and Taylor's physiological basis of medical practice. 12th ed. Williams & Wilkins; 1990.
[56] Berne Robert M, Levy Matthew N. Cardiovascular physiology. 4th ed. The C.V. Mosby Company; 1981.
[57] Boron Walter F, Boulpaep Emile L. Medical physiology: a cellular and molecular approach. Saunders; 2003.
[58] Nageh Maged F, Kopelen Helen A, Zoghbi William A, Quiñones Miguel A, Nahueh Sherif F. Estimation of mean right atrial pressure using tissue Doppler imaging. Am J Cardiol 1999;84:1448–51.
[59] Sohn D-W, Chai I-H, Lee D-J, Kim H-C, Kim Hyo-Soo, Oh B-H, et al. Assessment of mitral annulus velocity by Doppler tissue imaging in the evaluation of left ventricular diastolic function. J Am College Cardiol 1997;30:474–80.
[60] Granet I. Fluid mechanics. Prentice Hall; 1996.
[61] Bellhouse BJ. The fluid mechanics of heart valves. In: Bergel DH, editor. Cardiovascular fluid dynamics, vol. 1. Academic Press; 1972 [chapter 8].
[62] Korakianitis T, Shi Y. Effects of atrio-ventricular interaction and heart valve dynamics on human cardiovascular system response. Mechanical Engineering Department: University of Glasgow; 2005. Technical report UoG-CET-2005-03.